Supporting Information

Pulsed Electron Paramagnetic Resonance Experiments Identify the Paramagnetic Intermediates in the Pyruvate:Ferredoxin Oxidoreductase Catalytic Cycle

Andrei V. Astashkin[†], Javier Seravalli[‡], Steven O. Mansoorabadi[¶], George H. Reed[¶], and Stephen W. Ragsdale[‡*]

[†]*Department of Chemistry, University of Arizona, Tucson, Arizona · 85721-0041, and* [‡]*Department of Biochemistry, University of Nebraska, Lincoln, Nebraska 68588, and* [¶]*Department of Biochemistry, University of Wisconsin, Madison, WI 53726-4087*

Supplementary experimental data and simulations

1. Pulsed ELDOR experiment.

In our experiments a three-pulse ELDOR technique was used. The field sweeps obtained at the observation and pumping mw frequencies are shown in Fig. S1. The time-domain ELDOR trace is shown in Fig. S2.

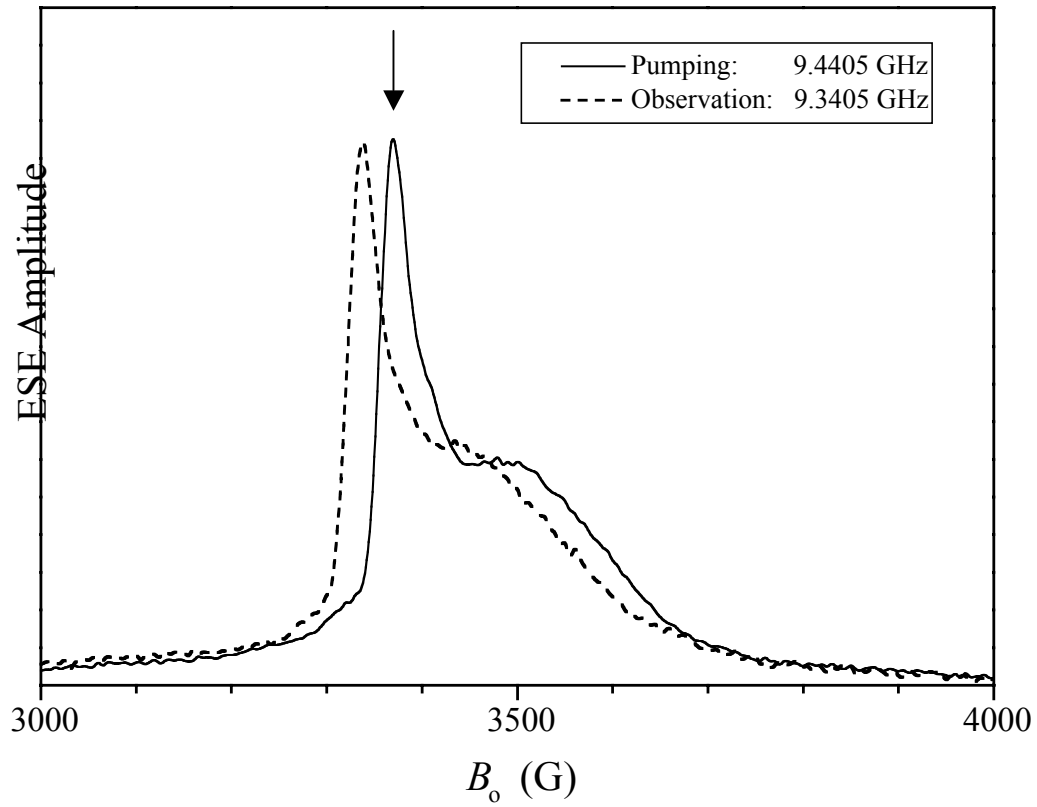

Figure S1. Two-pulse ESE field sweeps of PFOR obtained at the pumping and observation mw frequencies used in the pulsed ELDOR experiment. The narrow peak is due to the HE-TPP radical, while the broad feature is due to the $[4Fe\text{-}4S]^{1+}$ cluster. The arrow indicates the magnetic field position (B_o = 337 mT) used in the ELDOR experiment. Experimental conditions: mw frequencies, indicated in the Figure; mw pulses, 2 × 10 ns; time interval between the mw pulses, τ = 400 ns; temperature, 4.2 K.

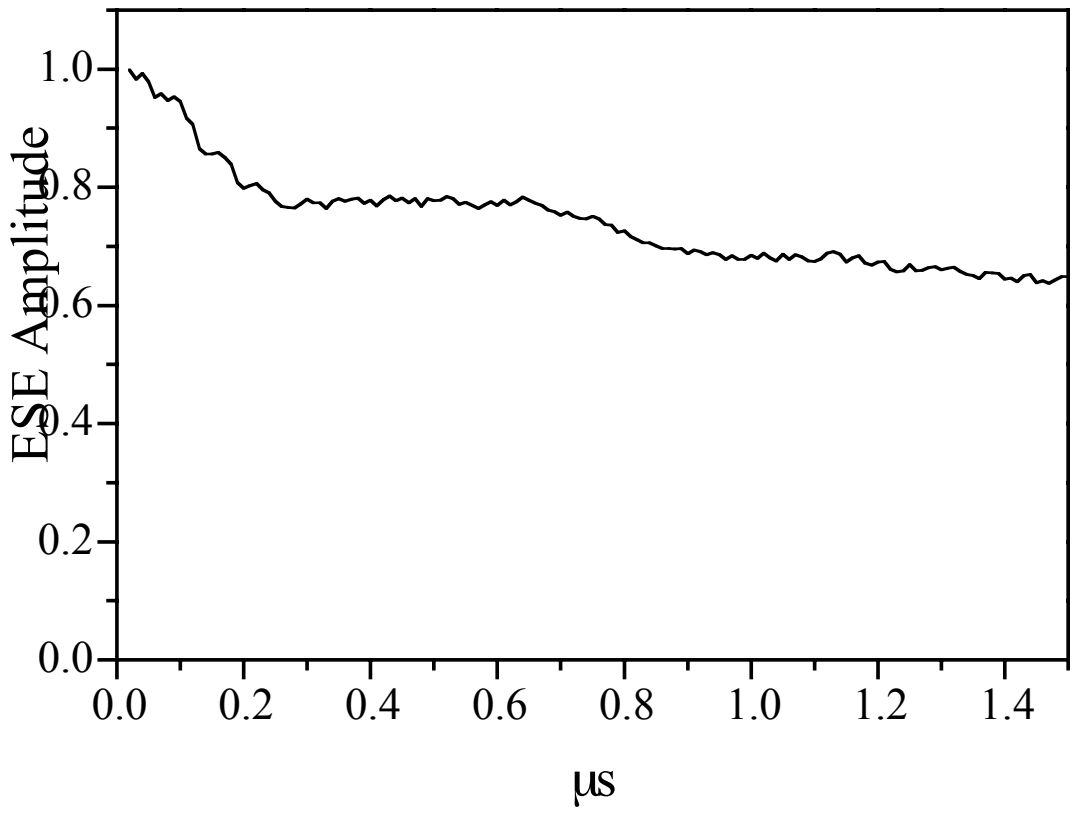

Figure S2. Three-pulse ELDOR trace. The low-frequency oscillation is due to the dipole interaction between $[4Fe\text{-}4S]^{1+}$ cluster and the HE-TPP radical within the same protein. The monotonous decay is due to the distant uniformly distributed HE-TPP radicals. Experimental conditions: observation mw frequency, 9.3405 GHz (in resonance with $[4Fe\text{-}4S]^{1+}$ cluster); pumping mw frequency, 9.4405 GHz (in resonance with HE-TPP radical); B_o = 337 mT; mw pulses, 3 × 15 ns; time interval between the observation mw pulses, τ = 1500 ns; temperature, 4.2 K.

2. RIDME experiment.

In order to decrease the dead time in the RIDME experiment, we used a refocused stimulated ESE technique with the pulse sequence (90°)-τ-(90°)-T-(90°)-τ+τ'-(180°)-τ'-ESE. In this experiment the variable time interval was τ, and we were observing the ESE modulation (ESEEM) on the signal of He-TPP radical caused by the longitudinal relaxation of $[4Fe\text{-}4S]^{1+}$ cluster spins during the fixed interval T. The experiment was performed at the temperatures of 13 K and 4.2 K. The relaxation rates of the cluster at these two temperatures were significantly different (see Fig. S3 showing the inversion recovery kinetics), which resulted in different contributions of the dipole interaction to the ESEEM and provided for the possibility to separate these contributions.

Fig. S4 shows the cosine FT spectra of the stimulated ESEEM traces obtained at 13 K and 4.2 K (solid and dashed traces 1) and their difference, the RIDME trace 2.

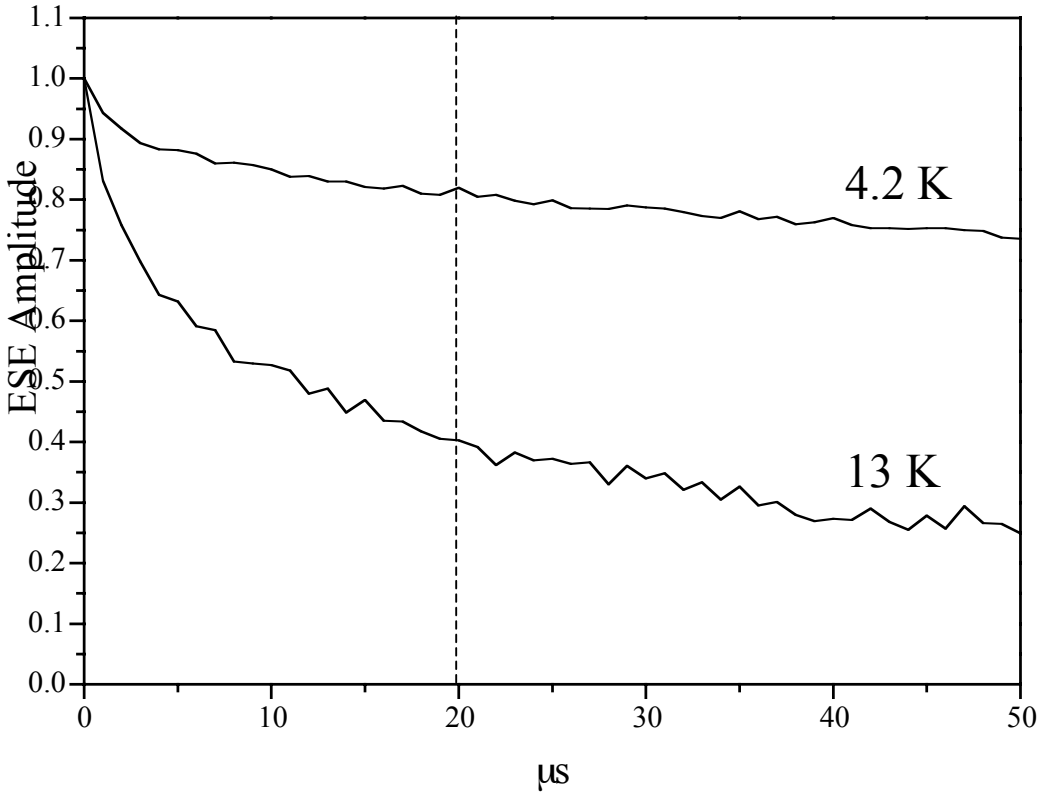

Figure S3. Inversion recovery traces for the 4Fe-4S cluster at two different temperatures For convenience of presentation the experimental ESE amplitudes were subtracted from the asymptotic value obtained without the inversion pulse, and then normalized by the amplitude at time $T \approx 0$ (actually, $T = 50$ ns) between the inversion pulse and the first observation pulse. Experimental conditions: mw frequency, 9.4405 GHz; B_o = 348.5 mT (in resonance with HE-TPP radical); inversion mw pulse length, 10 ns; observation mw pulses, 2 × 15 ns; time interval between the observation pulses, $\tau = 400$ ns.
Vertical dashed line shows the time between the 2nd and 3rd pulses in RIDME experiment. One can see that at 13 K the longitudinal relaxation of the FeS clusters resulted in about 60% reduction of the trace amplitude, while at 4.2 K the decrease was only about 18%.

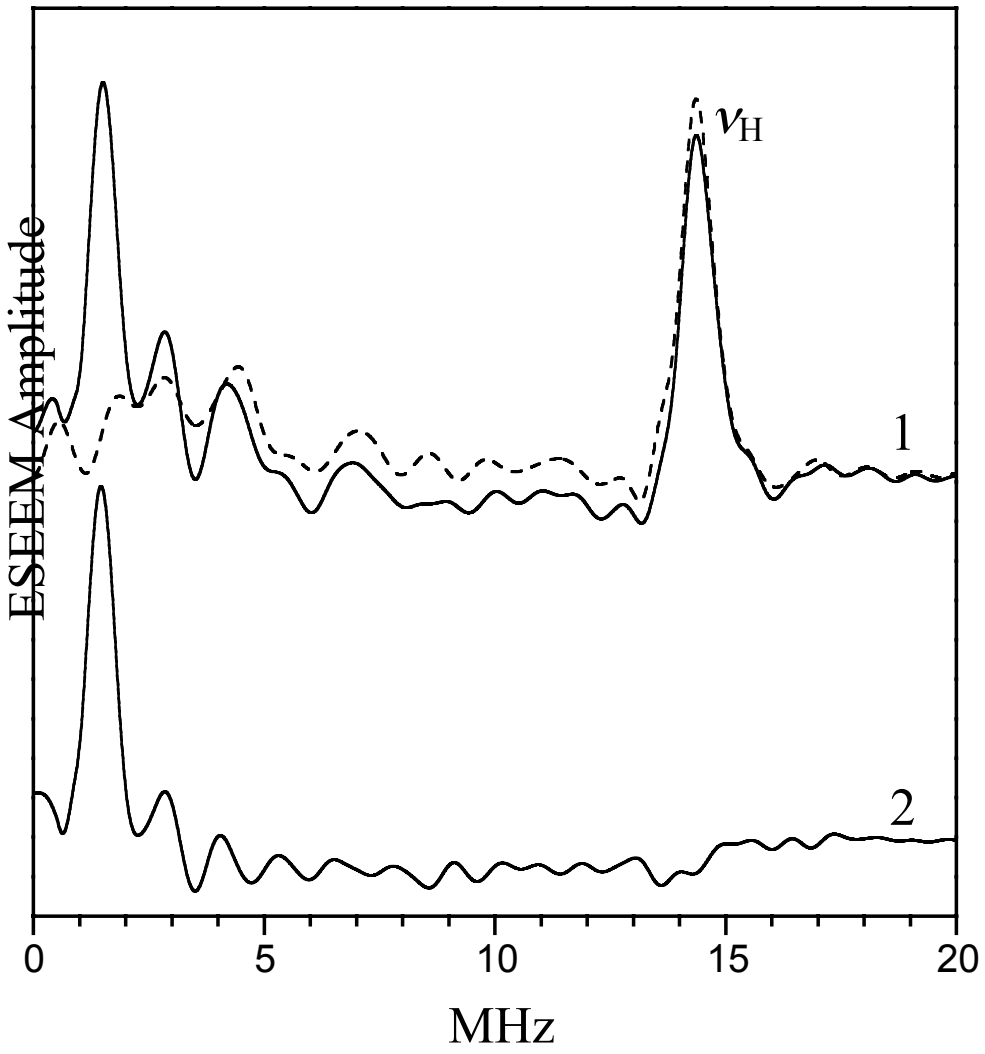

Figure S4. RIDME experiment based on a refocused stimulated ESE sequence (90°)-τ-(90°)-T-(90°)-τ+τ'-(180°)-τ'-ESE. Time intervals T and τ' are fixed, while τ is varied. The ESEEM is recorded as a function of τ. Solid trace 1, cosine FT of refocused stimulated ESEEM obtained at the temperature of 13 K. Dashed trace 1, the same at 4.2 K. Trace 2 is the RIDME spectrum obtained as a difference between solid and dashed traces 1. Experimental conditions: mw frequency, 9.4405 GHz; B_o = 337 mT; mw pulses, 3 × 15 ns (90°) + 1 × 10 ns (180°); T = 20 μs; τ' = 280 ns. The line marked ν_H in traces 1 is the transition line of distant protons (ν_H is the ^{1}H Zeeman frequency).

3. Numerical simulations of ELDOR and RIDME spectra.

The numerical simulations were performed assuming an axial dipole interaction tensor characterized by the dipolar coupling constant D_o. The dipole interaction for every orientation of the magnetic field was then calculated as $D = D_o[1-3\cos^2\theta]$ (where θ is the angle between $\mathbf{B_o}$ and the radius vector joining the radical with the cluster) and taken with the statistical weight of $\sin\theta$. At this stage we have considered the both paramagnetic species as point dipoles. Since no orientational dependence was expected in the RIDME experiment, more credibility was given to the RIDME spectrum than to the ELDOR one. The simulations have resulted in the range of possible D_o values from 1.62 ± 0.03 MHz. An example of simulation for D_o = 1.65 MHz is shown in Fig. S5.

As mentioned in the caption to Fig. S5, we have considered D_o to be statically Gaussian-distributed around the central value of 1.62 ± 0.03 MHz. The approximate distribution width (between the maximal slope points), ΔD = 0.3 MHz, was arrived at by comparing the time domain experimental oscillations with those simulated for various values of ΔD (see Fig. S6).

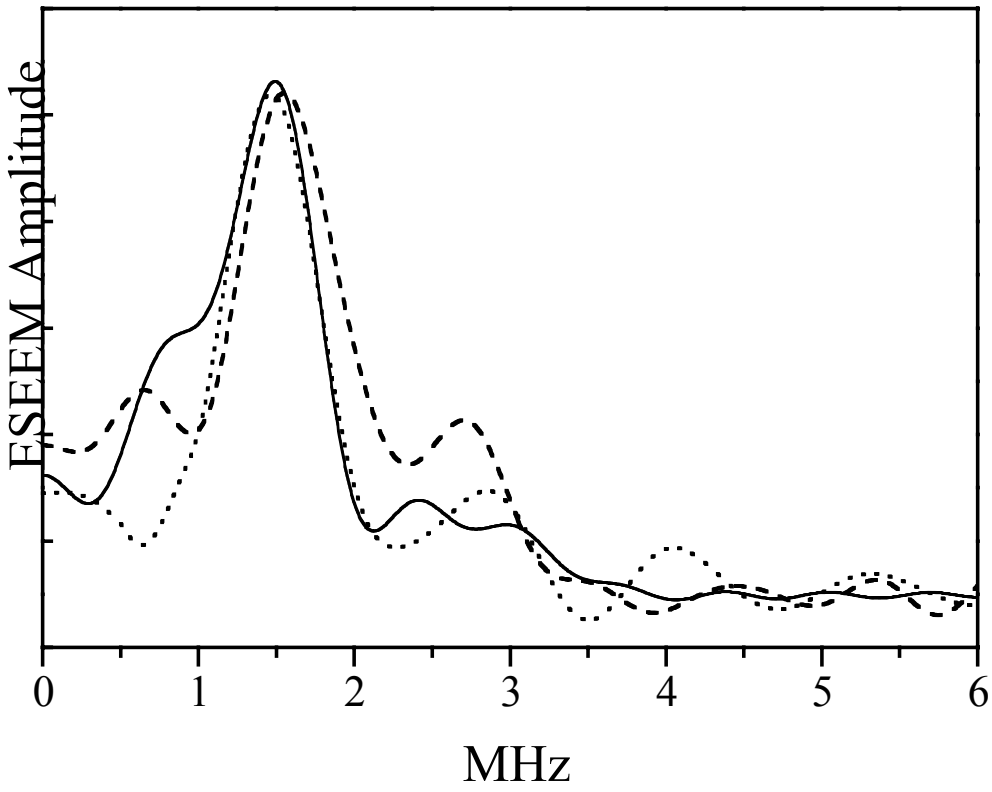

Figure S5. Dotted and dashed traces are, respectively, RIDME and ELDOR spectra obtained by cosine FT of the time domain traces. Solid trace is a cosine FT of dipolar ESEEM simulated for D_o = 1.65 MHz. D_o was considered to be Gaussian-distributed around this central value with the distribution width of 0.3 MHz.

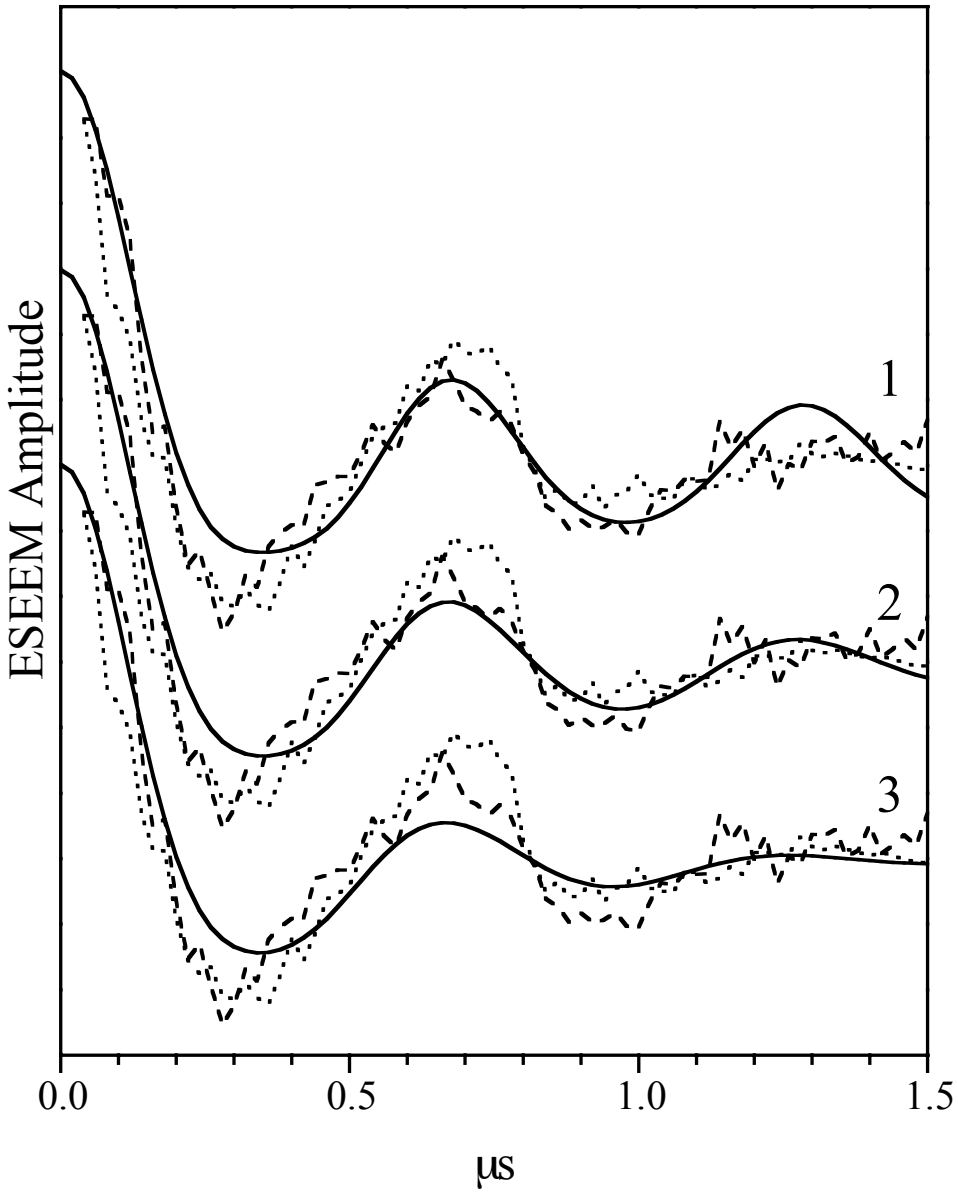

Figure S6. Dotted and dashed traces are, respectively, RIDME and ELDOR time domain traces. Solid traces are simulated for $2D_o$ = 3.3 MHz and ΔD = 0 MHz (trace 1), ΔD = 0.3 MHz (trace 2) and ΔD = 0.5 MHz (trace 3).

4. Analysis of the dipole interaction constant.

In a point dipole approximation the dipole interaction range of D_o = 1.62 ± 0.03 MHz translates into the range of effective distances R_{eff} ≈ 31.8 ± 0.2 Å (using $D_o = g_1 g_2 \beta^2 / R_{eff}^3$). However, since unpaired spin is delocalized both in the HE-TPP radical and in the $[4Fe\text{-}4S]^{1+}$ cluster, it is preferable to expand the point dipole approximation to better represent the delocalized spin [S0]. Elements of the dipole-dipole tensor can be calculated as a sum over all spin bearing atoms at the two paramagnetic centers as:

$$D_{ij} = \frac{\mu_o g^2 \beta^2}{4\pi} \sum_m \sum_n \rho_1^m \rho_2^n \frac{\left[\left| \vec{r}_2^{\,n} - \vec{r}_1^{\,m} \right|^2 \delta_{ij} - 3\left(\vec{r}_2^{\,n} - \vec{r}_1^{\,m}\right)_i \left(\vec{r}_2^{\,n} - \vec{r}_1^{\,m}\right)_j \right]}{\left| \vec{r}_2^{\,n} - \vec{r}_1^{\,m} \right|^5} \quad \textbf{(S1)}$$

where $\rho_1^m \rho_2^n$ and $\left| \vec{r}_2^{\,n} - \vec{r}_1^{\,m} \right|$ represent spin densities and inter-atomic vectors, respectively, of atoms *m* and *n* at centers 1 and 2 [S1]. The inter-atomic vectors were taken from the X-ray coordinates of PFOR [S2]. The spin densities were obtained from electronic structure calculations corrected for spin projection factors. The latter are summarized in Fig. S7.

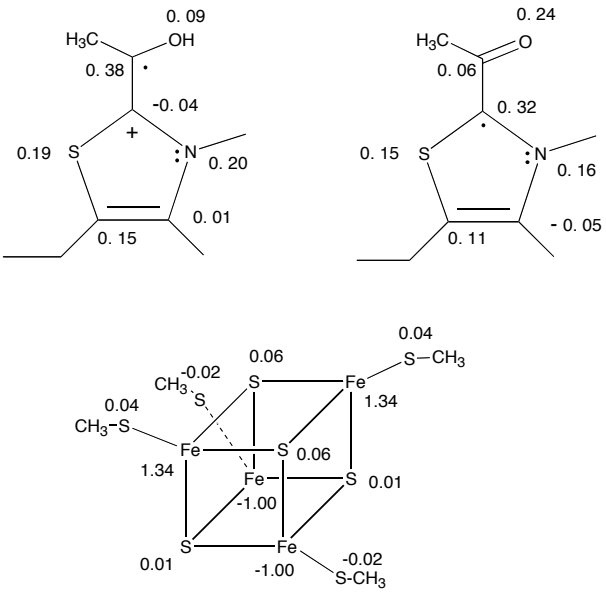

Figure S7. Spin densities in the protonated and neutral form of the HE-TPP radical and in the $[4Fe\text{-}4S]^{1+}$ cluster. Spin densities for the protonated and unprotonated forms of the HE-TPP radical were obtained from single point energy calculations on the optimized structures using *Gaussian98*. Geometry optimizations were performed using Becke-style 3-Parameter Density Functional Theory (DFT) with the Lee-Yang-Parr correlation functional (B3LYP) and Pople's polarized double-ζ 6-31G* basis set. Single-point calculations were performed using the B3LYP hybrid functional in combination with the DFT-optimized valence triple-ζ basis, TZVP. Spin densities for the pure $S = 1/2$ ground state of the $[4Fe\text{-}4S]^{1+}$ cluster were calculated from the spin densities of the broken symmetry (BS) state of the cluster taken from the paper by Torres *et al.* [S3]. The BS spin densities of the iron atoms were scaled by $|K_i/2S_i|$, were K_i is the site spin projection factor (11/6 and –4/3 for the mixed valence and ferrous irons, respectively) and S_i is the formal site spin (9/4 and 2 for the mixed valence and ferrous irons, respectively). The BS spin densities of the thiolate sulfur atoms and methyl groups were scaled by the same factor as the corresponding iron to which it is bonded and those of the bridging sulfur atoms were scaled by the average of the factors of the irons to which they are bonded.

Principal values of the calculated (eq. S1) dipole-dipole tensors are summarized in Table S1. Axial tensors are of the form (D_o, D_o, $-2D_o$). For the rhombic tensors, D_o is approximated by the average of the first two principal values. Values of D_o calculated for Cluster B for most of the possible positions of the valence delocalized pair of Fe's in the cluster approximate the experimentally determined value. Values calculated for Cluster A are uniformly too large, and values calculated for Cluster C are smaller than the experimentally determined value.

Table S1. Principal values of calculated dipole-dipole tensors of the HE-TPP radical (protonated and neutral) and the $[4Fe\text{-}4S]^{1+}$ of clusters A, B or C in PFOR. X-ray coordinates were from PDB code 1KEK. Spin densities are summarized in Fig. S7.

[a]Position of delocalized pair	Cluster	H^+-HE-TPP• (MHz)	HE-TPP• (MHz)
	A	25.6, 23.5, –49.1	24.7, 23.5, –48.1
1	**B**	**1.9, 1.8, –3.7**	**1.8, 1.8, –3.6**
	C	0.5, 0.4, –0.9	0.5, 0.4, -.9
	A	22.6, 22.1, –44.7	22.2, 21.6, –43.9
2	**B**	**1.4, 1.2, –2.6**	**1.4, 1.2, –2.5**
	C	0.6, 0.6, –1.2	0.6, 0.6, –1.2
	A	23.1, 19.9, –43.0	22.3, 19.9, –42.3
3	**B**	**1.1, 0.9, –1.9**	**1.0, 0.9, –1.9**
	C	0.3, 0.3, –0.6	0.3, 0.3, –0.6
	A	12.3, 1.8, –14.1	11.9, 1.5, –13.5
4	**B**	**1.6, 1.4, –3.0**	**1.5, 1.4, –2.9**
	C	0.6, 0.6, –1.2	0.6, 0.6, –1.2
	A	10.5, 0.1, –10.7	10.5, 0.2, –10.7
5	**B**	**1.2, 1.1, –2.3**	**1.2, 1.1, –2.3**
	C	0.3, 0.3, –0.6	0.3, 0.3, –0.6
	A	-6.4, –2.8, 9.2	-6.4, –2.7, 9.1
6	**B**	**0.5, 0.5, –1.0**	**0.5, 0.5, –1.0**
	C	0.5, 0.5, –1.0	0.5, 0.5, –0.9

[a] The six groups are for the six possible faces of each cluster that could contain the valence delocalized pair of Fe's in the $[4Fe\text{-}4S]^{1+}$ cluster [S4].

Acknowledgments. The authors thank Dr. L. Noodleman for his suggestions regarding calculating spin projection factors of the pure S=1/2 state of the $[4Fe\text{-}4S]^{1+}$ cluster.

References

S0. Mukai, K.; Sogabe, A., *J. Chem. Phys.* **1980,** *72,* 598-601.

S1. Mansoorabadi, S. O.; Reed, G. H. In *Paramagnetic Resonance of Metallobiomolecules,* Telser, J., Ed., American Chemical Society, Washington, D. C., 2003, Chapter 4.

S2. Chabriere, E.; Charon, M.-H.; Volbeda, A.; Pieulle, L.; Hatchikian, E. C.; Fontecilla-Camps, J.-C., *Nature Structural Biology* **1999,** 6, 182-190.

S3. Torres, R. A.; Lovell, T.; Noodleman, L., Case, D. A. *J. Am Chem. Soc.* **2003,** *125,* 1923-1936.

S4. Beinert, H.; Holm, R. H.; Münck, E. *Science* **1997**, *277*, 653-659.